Monte Carlo simulation of the "Kondo necklace"

R. T. Scalettar, D. J. Scalapino, and R. L. Sugar
Department of Physics, University of California, Santa Barbara, California 93106
(Received 14 January 1985)

The projector Monte Carlo method and finite-size scaling are applied to the solution of the ground-state properties of the "Kondo necklace" Hamiltonian. The energy and various spin-spin correlation functions are calculated for chains up to 16 sites in length. Correlations between the spins on different sites are evaluated, and the nature of the ground-state phase as a function of the ratio of the exchange coupling J to the bandwidth W is examined. Evaluation of the correlation function $\langle \mathbf{S}(i)\cdot\tau(i)\rangle$ shows that as the coupling between the localized S spins and the τ spin chain increases, the system becomes composed of independent singlets on each site. Contrary to both mean-field and various approximate renormalization-group calculations, we find that our results are consistent with an absence of magnetic order as soon as J is different from 0.

I. INTRODUCTION

There is considerable current interest in the Kondo lattice Hamiltonian,

$$H=\sum_{k,a} e(k)c_a^{\dagger}(k)c_a(k)+\sum_{i,a,b} c_a^{\dagger}(i)\sigma_{ab}c_b(i)\cdot\mathbf{S}_i \ , \tag{1}$$

as a model of concentrated magnetic sites coupled to conduction-band electrons. Extensive measurements of the specific heat, electric resistivity, and magnetic susceptibility of such compounds as $CeAl_2$ and $CeAl_3$ have been performed,[1] and a physical picture of their ground state is emerging. Focusing on their magnetic behavior, the object is to explain the anomalously low temperature for the onset of magnetic order in $CeAl_2$, and the apparent absence of order even at $T=0$ in $CeAl_3$, despite the presence of unpaired f orbitals. The physical picture suggested by Doniach[2] and others,[3] is that there is a competition between a magnetically ordered state arising from the Ruderman-Kittel-Kasuya-Yosida (RKKY) conduction-electron-mediated coupling between the local moments and a nonmagnetic Kondo singlet state in which the conduction electrons screen the local moments.

The "Kondo necklace,"

$$H=W\sum_i [\tau_x(i)\tau_x(i+1)+\tau_y(i)\tau_y(i+1)] +J\sum_i \tau(i)\cdot\mathbf{S}(i) \ , \tag{2}$$

has been proposed[2] as a simpler version of Eq. (1), which nevertheless retains the essential competition between magnetic ordering due to the indirect coupling of the S spins via the τ spins and the $J\mathbf{S}\cdot\tau$ driven singlet formation. There are, of course, some differences between the models. The "Kondo necklace," Eq. (2), neglects the conduction-electron-charge degrees of freedom. In addition, the effective coupling of the local S spins differs. For the Kondo lattice, one has in second-order perturbation theory the one-dimensional (1D) RKKY coupling

$$H_{\rm eff}=\sum_{i,j} J_z(i,j)S_z(i)S_z(j) +J_x(i,j)[S_x(i)S_x(j)+S_y(i)S_y(j)] \ , \tag{3}$$

with

$$J_z(i,j)=J_x(i,j)\sim\int_0^{\beta}\langle n(i,\tau)n(j,0)\rangle d\tau \ , \tag{4a}$$

and

$$\langle n(i,\tau)n(j,0)\rangle\sim\frac{1}{[\,|i-j|^2+V_f^2\tau^2]^{1/2}} \ . \tag{4b}$$

For the "Kondo necklace,"

$$J_z(i,j)\sim\int_0^{\beta}\langle\tau_z(i,\tau)\tau_z(j,0)\rangle d\tau \ , \qquad J_x(i,j)\sim\int_0^{\beta}\langle\tau_x(i,\tau)\tau_x(j,0)\rangle d\tau \ , \tag{5a}$$

and according to Luther and Peschel,[4]

$$\langle\tau_z(i,\tau)\tau_z(j,0)\rangle\sim\frac{1}{[\,|i-j|^2+V_f^2\tau^2]^{1}} \ , \qquad \langle\tau_x(i,\tau)\tau_x(j,0)\rangle\sim\frac{1}{[\,|i-j|^2+V_f^2\tau^2]^{1/4}} \ , \tag{5b}$$

for the XY model. Thus, the spatial decay of the effective couplings is anisotropic in the "Kondo necklace" case, and in addition the transverse coupling is anomalously long range. If a Heisenberg coupling $\tau(i)\cdot\tau(i+1)$ were taken instead of the XY term in Eq. (2), one would obtain

$$J_z=J_x\sim\int_0^{\beta}[\,|i-j|^2+V_f^2\tau^2]^{1/2}d\tau \ ,$$

corresponding to the second-order result Eq. (4b) for the Kondo lattice. This also restores the full rotational symmetry which was lost in going from Eq. (1) to Eq. (2). Despite the differences noted above, Doniach has observed[2] that the scaling behavior of the Hamiltonians (1) and (2) is identical in the one impurity case. Here we will treat the original "Kondo necklace" as given by Eq. (2).

It is useful to review briefly the results of previous stud-

ies of this model. Doniach's[2] original mean-field treatment used a variational ground state which is the product of two spin (τ,S) wave functions on each site. The energy is minimized subject to the variation of the triplet and singlet components. For ratios of the exchange coupling J to the bandwidth W greater than $(J/W)_c=1$, it was found that the ground state reduces to a product of singlet states on each site, while for J/W below this value, triplet components enter. The staggered magnetization order parameter $\langle(-1)^l S_x(l)\rangle$ was evaluated and found to behave as $[1-(J/W)^2]^{1/2}$ below $(J/W)_c$ and to be zero above $(J/W)_c$. Following this, Jullien, *et al.*[5] carried out an approximate real-space renormalization-group treatment and concluded, in agreement with the mean-field result, that the system has a second-order transition. End-to-end correlation functions such as $\langle S_+(1)S_-(2^N)\rangle$ were found to have nonzero values below $(J/W)_c=0.411$ in the large N limit, indicating the presence of long-range order. The energy was also evaluated and, depending upon the details of the procedure (e.g., the number of sites, two or four, per block), the energy for the $J=0$ case (XY model) was found to differ from the exact result by between 9 and 21%. Subsequent to this work, Jullien and co-workers[6] reported further real-space renormalization-group calculations in which the low J/W phase did not exhibit long-range order but was suggested to be XY in character. Hanke and Hirsch[7] reached similar conclusions using another approximate real-space renormalization procedure based on an odd number of sites per block. They found a critical point $(J/W)_c=0.375$ which separates the antiferromagnetic and Kondo regimes. They also evaluated the energy and obtain results which agree with the exact $J=0$ value to within 20%.

In the work reported here, we have used a Monte Carlo method described in Sec. II to study the N site "Kondo necklace," Eq. (2), with N ranging up to 16 sites. Extrapolating to $N\rightarrow\infty$ we find the ground-state energy for $0.0<J/W<2.0$ to within an estimated error of 0.5%. To within even sharper bounds the algorithm agrees with the exact two and four site solutions. In weak coupling, $J=0$, the "Kondo necklace" becomes the exactly soluble XY model. Energies and correlation functions for systems of up to 20 sites, generated by Monte Carlo methods, agree with exact results in this case. These quantities are also found to fit smoothly onto a strong coupling expansion generated for J/W large. On-site correlation functions are obtained. As J/W increases, $\langle S_z(i)\tau_z(i)\rangle$, $\langle S_x(i)\tau_x(i)\rangle$, and $\langle \mathbf{S}(i)\cdot\boldsymbol{\tau}(i)\rangle$ are shown to approach values consistent with the picture of independent singlet wave functions on each site. By studying the spatial dependence of the spin-spin correlation functions, we conclude that there is no long-range magnetic order in the ground state for any value of J/W. Furthermore, while there remains the possibility of a Kosterlitz-Thouless-like phase transition in which the correlations fall algebraically below some finite critical value of J/W, we find that our results are more consistent with the existence of a critical point at $J/W=0$. In this case, for all $J/W>0$, the antiferromagnetic correlations decay exponentially with a correlation length that diverges at $J/W=0$ where the "Kondo necklace" becomes the XY model, and correlations decay algebraically. Following a discussion of the calculational procedure, Sec. III contains our results and scaling analysis, and Sec. IV our conclusions.

II. TECHNIQUE

A. Basic procedure

In this work we use recently developed methods for the Monte Carlo simulation of quantum-spin and lattice-fermion systems.[8] These methods have been applied to the study of the Gross-Neveu model,[8] the Ising model,[9] the Peierls-Hubbard model,[10] and the calculation of string tension and roughening in lattice QED.[11] The operator $e^{-\beta H}$ is used to project out the lowest energy state of a given symmetry. The energy and expectation values of operators are given by

$$e^{-\Delta\beta E_0}=\lim_{\beta\rightarrow\infty}[\langle\chi|e^{-(\beta+\Delta\beta)H}|\phi\rangle/\langle\chi|e^{-\beta H}|\phi\rangle]\ , \quad (6a)$$

$$\langle\psi_0|Q|\psi_0\rangle = \lim_{\beta\rightarrow\infty}[\langle\chi|e^{-\beta H}Qe^{-\beta H}|\phi\rangle/\langle\chi|e^{-2\beta H}|\phi\rangle]\ . \quad (6b)$$

$|\phi\rangle$ and $|\chi\rangle$ are trial states whose choice is discussed in more detail below. The operator $e^{-\beta H}$ is applied by dividing β into L intervals of length $\Delta\tau$, where $\Delta\tau$ is small enough to allow the approximation

$$e^{-\Delta\tau(H_1+H_2+H_3)}\approx e^{-\Delta\tau H_1}e^{-\Delta\tau H_2}e^{-\Delta\tau H_3}\ .$$

Then, as we will see, this separation of H into various parts allows us to simply evaluate the relevant matrix elements. Complete sets of intermediate states are introduced and, following Kuti,[12,13] the matrix elements $\langle i|e^{-\Delta\tau H_k}|j\rangle$ are divided into elemental probabilities and scores,

$$\langle i|e^{-\Delta\tau H_k}|j\rangle=P_{ij}(k)S_{ij}(k)\ . \quad (7)$$

This breakup is arbitrary and can be adjusted to optimize convergence. As described in Blankenbecler and Sugar,[8] the probabilities are employed to generate the new configuration, i.e., if the system is in state $|i\rangle$, then $|j\rangle$ is chosen for the state at time $\Delta\tau$ later with probability $P_{ij}(k)$. The scores for each time slice are multiplied together to form a weight, and the expressions of interest are then approximated by the average of the weights over many trials

$$\langle\chi|e^{-\beta H}|\phi\rangle = \lim_{\text{number of trials}\rightarrow\infty}\langle\chi|i_{3L+1}\rangle Si_{3L+1}i_{3L}(3)\cdots\ . \quad (8)$$

It is important that the matrix elements be positive, since the probabilities must be positive, and averaging over scores that vary in sign engenders cancellations that introduce large statistical fluctuations. For this reason a rotation is performed on the Hamiltonian (2) to cast it into the form

$$H=-W\sum_i[\tau_x(i)\tau_x(i+1)+\tau_x(i)\tau_x(i+1)]$$
$$+J[S_z(i)\tau_z(i)-S_x(i)\tau_x(i)-S_y(i)\tau_y(i)]\ . \quad (9)$$

Next, the Hamiltonian Eq. (9) is divided up so that $H=H_1+H_2+H_3$ with

$$H_1=-W\sum_{i\ \text{odd}}[\tau_x(i)\tau_x(i+1)+\tau_y(i)\tau_y(i+1)]\ ,$$
$$H_2=J\sum_i[S_z(i)\tau_z(i)-S_x(i)\tau_x(i)-S_y(i)\tau_y(i)]\ , \quad (10)$$
$$H_3=-W\sum_{i\ \text{even}}[\tau_x(i)\tau_x(i+1)+\tau_y(i)\tau_y(i+1)]\ .$$

It is seen that H_1, H_2, and H_3 are each composed of a sum of mutually commuting pieces. The application of the operators $e^{-\Delta\tau H_k}$ to the lattice of spins then involves only solving independent two-site problems. Because we are interested in the question of magnetic order in the X-Y plane, it is convenient to work in the $(\tau_x S_x)$-diagonal representation. If one works in the $(\tau_z S_z)$-diagonal representation, the Monte Carlo calculation of nondiagonal correlation is considerably more time consuming and subject to larger statistical fluctuations.[14] The reason is that to calculate any operator ground-state expectation value, according to Eq. (6b) we first project from 0 to β, generating a product of scores. We then apply the operator. If it is diagonal, this just yields a number and leaves the state at β unchanged, We then project from β to 2β and obtain the remaining scores. Since the state is unchanged in applying a diagonal operator, the same sequence of scores can be used in the denominator of Eq. (6b). If the operator were not diagonal, only the scores from 0 to β could be shared, since the states at β before and after the operator acts are now different and must be propagated separately from β to 2β. The advantage in evaluating a diagonal operator is not only the obvious time saved, but also that the use of the same set of scores in numerator and denominator reduces statistical fluctuations.

The matrix elements for the above division of the Hamiltonian are

$$e^{-\Delta\tau H_1}|++\rangle=e^{a}[\cosh(a)|++\rangle+\sinh(a)|--\rangle]\ ,$$
$$e^{-\Delta\tau H_1}|--\rangle=e^{a}[\sinh(a)|++\rangle+\cosh(a)|--\rangle]\ , \quad (11a)$$
$$e^{-\Delta\tau H_1}|+-\rangle=e^{-a}[\cosh(a)|+-\rangle+\sinh(a)|-+\rangle]\ ,$$
$$e^{-\Delta\tau H_1}|-+\rangle=e^{-a}[\sinh(a)|+-\rangle+\cosh(a)|-+\rangle]$$

[with $|++\rangle=|\tau_x(i)=+\frac{1}{2},\ \tau_x(i+1)=+\frac{1}{2}\rangle$, and $a=W\Delta\tau/4$], and similarly for H_3. For H_2,

$$e^{-\Delta\tau H_2}|++\rangle=e^{-b}|++\rangle,\ H_2|--\rangle=e^{-b}|--\rangle\ ,$$
$$e^{-\Delta\tau H_2}|+-\rangle=e^{b}[\cosh(2b)|+-\rangle+\sinh(2b)|-+\rangle]\ , \quad (11b)$$
$$e^{-\Delta\tau H_2}|-+\rangle=e^{b}[\sinh(2b)|+-\rangle+\cosh(2b)|-+\rangle]$$

[with $|++\rangle=|\tau_x(i)=+\frac{1}{2},\ S_x(i)=+\frac{1}{2}\rangle$, and $b=J\Delta\tau/4$]. The lattice is chosen to have N sites, and the boundary conditions are chosen so that the above formulas hold for the link connecting the first and Nth sites, i.e., periodic for $N=2,6,10,\ldots$ and antiperiodic for $N=4,8,12,\ldots$.

Frequently the simplest division of the matrix element into probability and score is adequate. For example, for $\exp(-\Delta\tau H_1)$ in Eq. (11a),

$$P(|++\rangle\rightarrow|++\rangle)=\cosh(a)/[\sinh(a)+\cosh(a)]\ ,$$
$$S(|++\rangle\rightarrow|++\rangle)=e^{a}[\cosh(a)+\sinh(a)]\ . \quad (12)$$

However, for J/W small, we expect considerable correlations between neighboring τ spins. It is generally found that convergence is improved by examining $\tau_x(i-1)$ and $\tau_x(i+2)$ and modifying the probabilities and scores appropriately. For example, if they are both $+$, we may enhance $P(|++\rangle\rightarrow|++\rangle)$. Of course, we must add a compensating factor to the score to keep the product of probability and score, the matrix element, unchanged. Similarly for large J/W, convergence rates are improved by adjusting the probabilities to favor moves to states where the τ and S spins are antialigned. Again choosing H_1 as an example, we may increase $P(|++\rangle\rightarrow|--\rangle)$ if both $S_x(i)$ and $S_x(i+1)$ are $+$ and decrease the corresponding score S keeping PS constant. In any event, it should be emphasized that while this procedure provides an opportunity to insert some intuition concerning the physics into the algorithm, the results are consistent with each other for different divisions of the matrix element. Only the rate of convergence, not the final value is affected.

It is worthwhile to mention that the trial state $|\phi\rangle$ can also be chosen to optimize convergence. Usually $|\chi\rangle$ is chosen to be the broad state

$$|\chi\rangle=\frac{1}{\sqrt{N}}\sum_{\{|\lambda\rangle\}}|\lambda\rangle$$

summed over all states $|\lambda\rangle$ so that the final quantity $\langle\chi|i_{3N+1}\rangle$ in Eq. (8) has the trivial value $1/\sqrt{N}$, and need not be calculated explicitly. The closer $|\phi\rangle$ is to the ground state to begin with, the smaller β can be. $|\phi\rangle$ can thus be chosen to be the result of some variational calculation of the ground state. More simply, we might choose $|\phi\rangle$ to have considerable correlations between spins when J/W is small, while for J/W large we might choose states with S and τ on each site antialigned. As before, it is verified that different choices for $|\phi\rangle$ give the same results to within statistical fluctuations.

As discussed in Kung *et al.*, it is often useful to employ a slight modification of the basic technique described above.[9,15] Up to now we have imagined that single configurations, chosen with a probability given by their matrix element with a trial state, are individually evolved employing the elemental probabilities P_{ij} and the resulting product of scores S_{ij} recorded. In the modified procedure which we will use here, a "population" of configurations is evolved. Suppose $|i\rangle$ were a configuration in the population. After a time step $\Delta\tau$, a new configuration $|j\rangle$ is generated with probability P_{ij} and score S_{ij}. (Actually, of course, many probabilities and scores are really involved in even a single time step since many two-site pairs are

TABLE I. Comparison of Monte Carlo results and exact diagonalization for $N=2$ sites. Errors quoted in the tables, and in the figures and text, are obtained from $[\sum_{i=1}^{N_T}(x_i-\bar{x}_i)^2]^{1/2}=(N_T)^{1/2}\sigma$, where i labels independent trials.

J/W	$-E_0$		$-c_{sx}(1)=-c_{tx}(1)$		c_{stx}		$-c_{sz}(1)=-c_{tz}(1)$		$-c_{stz}$		$-\mathbf{s}\cdot\boldsymbol{\tau}$	
0.00	0.5000(00)	0.5000	0.2500(00)	0.2500	0.0000(00)	0.0000	0.2500(00)	0.2500	0.0000(00)	0.0000	0.0000(00)	0.0000
0.05	0.5029(08)	0.5033	0.2484(13)	0.2482	0.0268(13)	0.0274	0.2472(04)	0.2471	0.0173(23)	0.0151	0.0709(30)	0.0699
0.10	0.5144(06)	0.5144	0.2400(10)	0.2411	0.0589(21)	0.0588	0.2371(01)	0.2373	0.0344(19)	0.0357	0.1522(25)	0.1533
0.15	0.5341(01)	0.5343	0.2307(19)	0.2305	0.0927(17)	0.0917	0.2195(11)	0.2200	0.01601(24)	0.0608	0.2435(41)	0.2442
0.20	0.5629(12)	0.5633	0.2146(15)	0.2148	0.1218(18)	0.1230	0.1971(12)	0.1968	0.0880(18)	0.0881	0.3349(27)	0.3341
0.25	0.6010(05)	0.6008	0.1972(12)	0.1968	0.1509(26)	0.1501	0.1710(08)	0.1712	0.1151(07)	0.1145	0.4159(27)	0.4147
0.30	0.6469(07)	0.6457	0.1777(14)	0.1784	0.1722(24)	0.1718	0.1451(13)	0.1460	0.1379(17)	0.1379	0.4817(23)	0.4815
0.35	0.6960(04)	0.6966	0.1612(18)	0.1612	0.1885(24)	0.1885	0.1239(18)	0.1235	0.1578(20)	0.1575	0.5430(19)	0.5345
0.40	0.7518(18)	0.7523	0.1454(08)	0.1458	0.2010(19)	0.2011	0.1042(13)	0.1043	0.1730(15)	0.1734	0.5751(28)	0.5756
0.45	0.8115(13)	0.8115	0.1327(11)	0.1324	0.2101(10)	0.2106	0.0884(21)	0.0884	0.1858(14)	0.1861	0.6072(15)	0.6073
0.50	0.8736(11)	0.8735	0.1201(19)	0.1209	0.2177(13)	0.1278	0.0756(20)	0.0754	0.1967(12)	0.1962	0.6327(13)	0.6318
0.60	1.0042(06)	1.0035	0.1022(16)	0.1023	0.2268(05)	0.2275	0.0571(14)	0.0560	0.2105(05)	0.2108	0.6641(07)	0.6658
0.70	1.1403(05)	1.1390	0.0879(14)	0.0884	0.2373(12)	0.2335	0.0426(21)	0.0428	0.2202(11)	0.2203	0.6870(09)	0.6873
0.75	1.2085(18)	1.2081	0.0821(12)	0.0827	0.2355(08)	0.2356	0.0368(17)	0.0379	0.2234(07)	0.2239	0.6944(11)	0.6951
1.00	1.5633(16)	1.5624	0.0626(23)	0.0623	0.2424(09)	0.2420	0.0231(22)	0.0222	0.2348(12)	0.2349	0.7196(15)	0.7189

separately evolved.) We compare S_{ij} with an average score S_{av} by computing $r=S_{ij}/S_{\text{av}}$, and if $0<r<1$, keep $|j\rangle$ with probability r; if $1<r<2$, always keep one copy of $|j\rangle$ and make a second with probability $r-1$; if $2<r<3$, always keep two copies of $|j\rangle$ and make a third with probability $r-2$ etc. This extra "copying factor" has modified the elemental probability P_{ij} of generating $|j\rangle$ from $|i\rangle$. It must be removed from the score. The

TABLE II. Comparison of Monte Carlo results and exact diagonalization for $N=4$ sites.

J/W	$-E_0$		$c_{tx}2$		$c_{sx}2$		$-\mathbf{s}\cdot\boldsymbol{\tau}$	
0.00	0.7078(05)	0.7071	0.1251(08)	0.1250	0.2500(00)		0.0056(39)	0.0000
0.05	0.7101(03)	0.7109	0.1249(16)	0.1250	0.1802(55)	0.1538	0.0751(49)	0.0772
0.10	0.7224(06)	0.7226	0.1247(13)	0.1248	0.1580(41)	0.1507	0.1568(35)	0.1553
0.15	0.7413(07)	0.7417	0.1248(09)	0.1242	0.1461(27)	0.1464	0.2250(46)	0.2253
0.20	0.7670(14)	0.7673	0.1222(14)	0.1228	0.1423(16)	0.1415	0.2870(33)	0.2855
0.25	0.7991(03)	0.7983	0.1201(17)	0.1205	0.1388(14)	0.1359	0.3357(41)	0.3346
0.30	0.8339(08)	0.8340	0.1173(09)	0.1172	0.1291(17)	0.1298	0.3788(28)	0.3786
0.35	0.8732(08)	0.8739	0.1134(12)	0.1130	0.1246(23)	0.1231	0.4201(24)	0.4181
0.40	0.9166(04)	0.9175	0.1062(15)	0.1077	0.1155(32)	0.1158	0.4532(30)	0.4543
0.45	0.9643(12)	0.9464	0.1021(7)	0.1018	0.1084(28)	0.1082	0.4863(27)	0.4875
0.50	1.0141(15)	1.0149	0.0944(08)	0.0953	0.0997(24)	0.1004	0.5191(24)	0.5180
0.60	1.1207(09)	1.1239	0.0829(17)	0.0818	0.0883(32)	0.0851	0.5697(18)	0.5695
0.70	1.2418(18)	1.2420	0.0685(14)	0.0690	0.0721(29)	0.0711	0.6083(21)	0.6100
0.75	1.3010(16)	1.3039	0.0632(16)	0.0632	0.0645(23)	0.0649	0.6271(14)	0.6262
1.00	1.6327(13)	1.6320	0.0391(13)	0.0410	0.0433(21)	0.0416	0.6790(12)	0.6796

J/W	$c_{tx}(1)$		$c_{sx}(1)$		$-c_{stx}$		$-c_{stz}$	
0.00	0.1768(12)	0.1758	0.2500(00)		0.000(00)	0.0000	0.0000(00)	0.0000
0.05	0.1753(23)	0.1758	0.2284(61)	0.1709	0.0388(25)	0.0370	0.0081(21)	0.0082
0.10	0.1734(19)	0.1729	0.1702(47)	0.1687	0.0666(38)	0.0675	0.0220(17)	0.0202
0.15	0.1688(14)	0.1685	0.1650(26)	0.1650	0.0938(26)	0.0954	0.0339(22)	0.0347
0.20	0.1630(17)	0.1634	0.1598(19)	0.1606	0.1179(19)	0.1171	0.0504(18)	0.0502
0.25	0.1589(22)	0.1577	0.1551(23)	0.1556	0.1345(17)	0.1344	0.0666(15)	0.0600
0.30	0.1521(38)	0.1517	0.1510(18)	0.1500	0.1477(21)	0.1484	0.0808(17)	0.0818
0.35	0.1452(18)	0.1453	0.1437(14)	0.1440	0.1621(15)	0.1604	0.0981(08)	0.0973
0.40	0.1382(19)	0.1385	0.1375(25)	0.1376	0.1710(10)	0.1709	0.1127(09)	0.1124
0.45	0.1318(24)	0.1314	0.1322(16)	0.1307	0.1804(14)	0.1804	0.1265(13)	0.1268
0.50	0.1267(21)	0.1243	0.1261(18)	0.1237	0.1862(11)	0.1888	0.1394(10)	0.1403
0.60	0.1108(32)	0.1101	0.1106(21)	0.1098	0.2033(13)	0.2029	0.1646(07)	0.1639
0.70	0.0984(30)	0.0970	0.0978(38)	0.0968	0.2140(08)	0.2137	0.1822(08)	0.1826
0.75	0.0918(29)	0.0911	0.0902(20)	0.0910	0.2178(14)	0.2180	0.1897(10)	0.1902
1.00	0.0747(25)	0.0682	0.0701(17)	0.0681	0.2324(11)	0.2320	0.2153(07)	0.2156

TABLE III. Comparison of Monte Carlo results and exact diagonalization for $J=0$ and $N=2,4,\ldots,16$ sites.

	$N=2$		$N=4$		$N=6$		$N=8$	
E_0	0.5000(00)	0.5000	0.7081(12)	0.7071	0.6664(15)	0.6667	0.6542(21)	0.6533
$c_{tx}(1)$	0.2500(00)	0.2500	0.1790(13)	0.1768	0.1679(17)	0.1667	0.1658(29)	0.1633
$c_{tx}(2)$			0.1259(11)	0.1250	0.1138(20)	0.1111	0.1119(18)	0.1067
$c_{tx}(3)$					0.1117(19)	0.1111	0.1024(22)	0.0986
$c_{tx}(4)$							0.0940(25)	0.0911
	$N=10$		$N=12$		$N=14$		$N=16$	
E_0	0.6476(28)	0.6572	0.6464(27)	0.6440	0.6433(25)	0.6420	0.6418(32)	0.6407
$c_{tx}(1)$	0.1627(17)	0.1617	0.1590(21)		0.1600(27)			
$c_{tx}(2)$	0.1047(18)	0.1047	0.1024(26)		0.1050(25)			
$c_{tx}(3)$	0.0938(27)	0.0936	0.0882(31)		0.0923(29)			
$c_{tx}(4)$	0.0821(26)	0.0838	0.0757(29)		0.0772(34)			
$c_{tx}(5)$	0.0816(33)	0.0838	0.0718(32)		0.0761(37)			
$c_{tx}(6)$			0.0665(30)		0.0714(41)			
$c_{tx}(7)$					0.0673(38)			

effect of this procedure is to make the scores for the different configurations in the population equal since

$$P_{ij}\rightarrow P_{ij}r\ ,$$
$$S_{ij}\rightarrow S_{ij}/r=S_{\mathrm{av}}\ .$$

Such a procedure minimizes statistical fluctuations.[9,15] Indeed, for this problem, this is found to be the case. The average score is updated at each time step by the ratio of the new population size to the old one to stabilize the number of configurations. Typically to generate the data presented below, configurations of size $250*N$ were evolved for between 10 and 100 independent trials. Care was taken to ensure that β was sufficiently large to project out the ground state by looking at the β dependence of the results. Similarly, it was verified that $\Delta\tau$ was sufficiently small. Usually $\beta=N/2$ and $\Delta\tau=0.25$ were chosen.

III. DETAILED RESULTS

The Hamiltonian (9) was studied first for several exactly soluble limits. For the purpose of describing the magnetic order in the system, it is useful to introduce the correlation functions

$$c_{tx}(l)=\langle\tau_x(i)\tau_x(i+l)\rangle\ ,$$
$$c_{sx}(l)=\langle S_x(i)S_x(i+l)\rangle\ , \qquad (13)$$
$$c_{stx}=\langle S_x(i)\tau_x(i)\rangle\ ,$$

and similarly for x replaced by z. In Tables I and II, Monte Carlo values for the ground-state energy and correlation functions are compared with exact diagonalization of the two and four-site cases. This provides one test that the program accurately calculates in all regimes of J/W. In Table III the results for $c_{tx}(l)$ and E_0 are compared with exact values in the weak coupling ($J=0$) case with $N=2,4,6,8,10$. This provides a partial check of the algorithm for larger systems. A further check is provided by the strong coupling expansion described below.

It is interesting to note several exact results that are borne out in the Monte Carlo simulation. The correlation function $c_{tx}(N/2)$ falls to zero as N increases at $J=0$ (Table III). It also must be zero in the large J limit since the Hamiltonian then describes N independent sites. [More precisely, in strong coupling, the first contribution to $c_{tx}(l)$ goes as $(W/J)^l$, which clearly goes to zero for J large and $l\rightarrow\infty$.] Finally, the effect of increasing J, when $N=2,4$, appears to be to decrease $c_{tx}(N/2)$ mono-

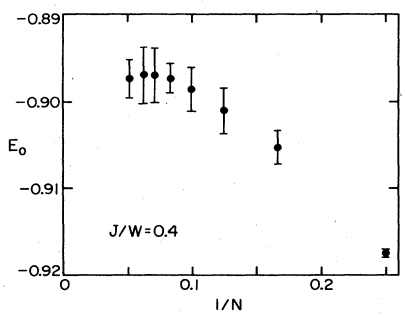

FIG. 1. Ground-state energy as a function of $1/N$ for a typical value $J/W=0.4$. For $N\gtrsim 10$, a well defined $N\rightarrow\infty$ result has been attained.

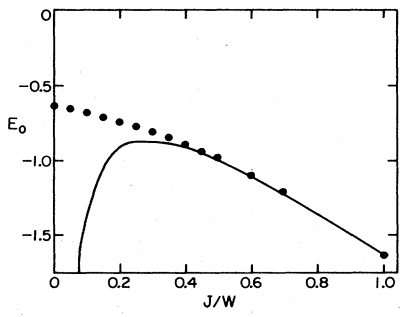

FIG. 2. $N\rightarrow\infty$ extrapolated value of ground state energy versus J/W. The strong coupling curve Eq. (14) is shown. The $J=0$ Monte Carlo value is -0.6361 ± 0.0012, and the exact $J=0$ (XY model) result is $-2/\pi=-0.6336$.

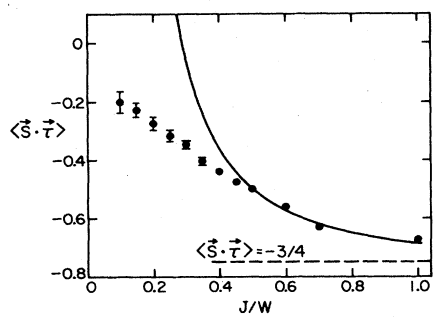

FIG. 3. $N\to\infty$ extrapolated value of $\langle \mathbf{S}(i)\cdot\tau(i)\rangle$ versus J/W. The strong coupling curve is shown. For large J/W two spins have condensed into singlets $\langle \mathbf{S}(i)\cdot\tau(i)\rangle = -\frac{3}{4}$ on each site.

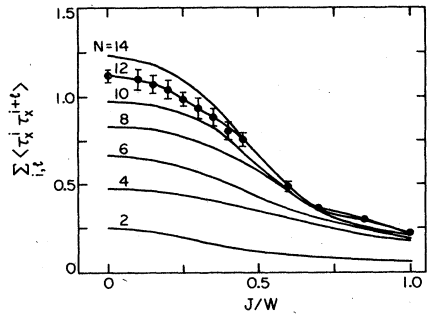

FIG. 5. $\mathscr{C}_{tx}^{(N)}$ versus J/W for $N=2,4,6,8,10,12,14$. For large J/W, $\mathscr{C}_{tx}^{(N)}$ is independent of N, while for small J/W, $\mathscr{C}_{tx}^{(N)}$ increases with N, showing the effect of a finite-size lattice.

tonically from its $J=0$ value. These three facts suggest that the correlation function at maximum separation $c_{tx}(N/2)$ falls to zero for all J in the large N limit, i.e., there is no magnetization in any regime of J/W. This may appear obvious since Eq. (9) is a one-dimensional Hamiltonian possessing a continuous symmetry. However, a perturbation theory in J/W shows there is a long-range effective coupling Eq. (5b) between the S spins which might allow the existence of long-range order. It should be mentioned that the effective Hamiltonian Eq. (3) with the $J_x(i,j)$ coupling given in Eq. (5b) is no longer thermodynamic, while the original Hamiltonian obviously is. This clearly shows that perturbation theory fails and would be consistent with the occurrence of a critical point at $J=0$.

Following these tests, the Monte Carlo analysis was extended to chains of 6, 8, 10, 12, 14, and 16 sites and nontrivial values of the parameters J and W. The ground-state energy for $J/W=0.4$ is shown as a function of $1/N$ in Fig. 1. The results have approached a well defined infinite system result for $N\gtrsim 10$ sites. These continuum values of E_0 are shown versus J/W in Fig. 2. The Monte Carlo calculation gives the correct $N\to\infty XY$ result at $J=0$, $E_0=-2/\pi$, as well as joining smoothly with the strong coupling expansion,

$$E_0/N = -\frac{3J}{4}\left[1+\frac{1}{3}\left[\frac{W}{J}\right]^2+\cdots\right], \tag{14}$$

which is shown as the smooth curve in Fig. 2.

The ground state expectation value of $\mathbf{S}(i)\cdot\tau(i) = 2c_{stx}+c_{stz}$ is shown in Fig. 3. It also has approached a well-defined result for $N=12,14,16$. In accordance with the physical picture suggested above, as J/W increases $\langle \mathbf{S}(i)\cdot\tau(i)\rangle$ approaches the limiting value $-\frac{3}{4}$ appropriate for a singlet wave function on each site. It, however, approaches this value smoothly, and cannot be used to extract information concerning critical properties.

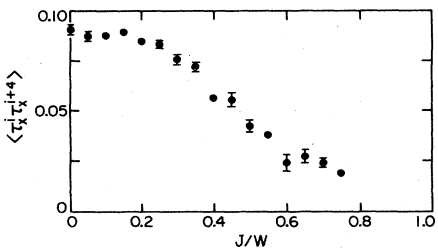

FIG. 4. $\langle \tau_x(i)\tau_x(i+4)\rangle$ versus J/W for $N=8$ sites.

Instead the correlation functions, $c_{tx}(l)$ and $c_{sx}(l)$ given in Eq. (13) are examined. In Fig. 4 we show $\langle \tau_x(i)\tau_x(i+4)\rangle$ versus J/W for $N=8$ sites. Because of our use of periodic boundary conditions, $N/2$ sites is the furthest separation of any two spins on the chain. Note that as J/W increases, the correlation function $\langle \tau_x(i)\tau_x(i+4)\rangle$ decreases. As N increases $\langle \tau_x(i)\tau_x(i+N/2)\rangle$ does not approach a well-defined value, but rather falls to zero for all J/W, clearly indicating the lack of long-range order. The $Q=0$ magnetic structure factors[16]

$$\mathscr{C}_{tx}^{(N)} = \sum_{l=1}^{N} c_{tx}(l)\,,$$
$$\mathscr{C}_{sx}^{(N)} = \sum_{l=1}^{N} c_{sx}(l) \tag{15}$$

are shown in Fig. 5 for $N=8,10,12,\ldots$ for various values of J/W. As J/W decreases below 0.5, finite-size lattice effects are clearly evident. Fits to the data for $J/W>0.4$ show the decay is exponential. In order to analyze further the magnetic structure factor data shown in Fig. 5, we note that according to finite-size scaling

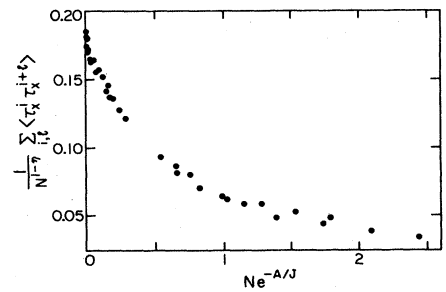

FIG. 6. Finite-size scaling is applied to the data of Fig. 5. $\mathscr{C}_{tx}^{(N)}/N^{(1-\eta)}$ is plotted versus $Ne^{-A/J}$. The values for different N now form a fairly well defined scaling curve.

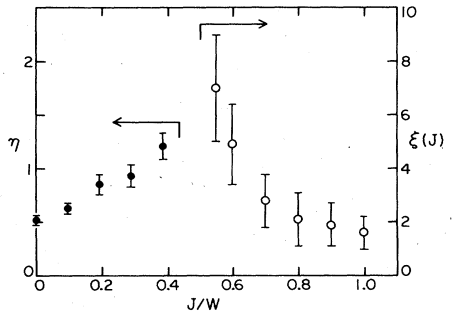

FIG. 7. Data of Fig. 5 is fit to an algebraic decay below $(J/W)_c$ and to an exponential decay above. The resulting power η is shown for $J/W<(J/W)_c$ and the correlation length for $J/W>(J/W)_c$.

$$\mathcal{C}_{tx}^{(N)}=\sum_{l=1}^{N} c_{tx}(l)\rightarrow \int_1^N \frac{e^{-l/\xi}}{l^{\eta}}dl = N^{1-\eta} f\left[\frac{N}{\xi}\right]. \quad (16)$$

Figure 6 shows the data of Fig. 5 replotted as $\mathcal{C}_{tx}^{(N)}/[N^{1-\eta}]$ versus N/ξ with $\eta=0.5$ to agree with the $J=0$ XY result and ξ assumed to vary as $\exp(A/J)$. In this plot $A=3$, but somewhat larger values of A also give similar quality fits. In addition, we could not rule out prefactors such as $\sqrt{J}\exp(A/J)$ or in fact some power-law divergence of ξ such as $\xi\sim 1/J^2$. Nevertheless, the structure-factor data is consistent with a $J=0$ critical point and a correlation length (or gap) which onsets as an essential singularity similar to the Hubbard model.

An alternative possibility which we also considered is that the critical point occurs at a finite value of J/W and is XY-like in character. In this case above the critical point, in the Kondo singlet regime, the magnetic correlations decay exponentially while at values of J/W less than the critical value the magnetic correlations have a power-law decay. Adopting this view, Fig. 5 would be interpreted as indicating the existence of a phase transition at finite (J/W) to a regime of algebraic decay. In order to extract a numerical value for the power of the algebraic falloff below $(J/W)_c$ we fit a plot of $\ln[c_{tx}(N/2)]$ versus $\ln(N)$ to a straight line. This turned out to be preferred to looking at $c_{tx}(l)$ for a fixed system size N and different l because of the complications introduced by the use of periodic boundary conditions. The resulting value of η for the power of the decay below the value $(J/W)_c=0.4$ estimated from Fig. 5 are shown in Fig. 7. Above $(J/W)_c$ we show the correlation length $\xi(J)$ for the exponential decay in that regime. At $J=0$ we find $\eta=+0.525(30)$ in reasonable agreement with the exact XY result, $+0.500$. However, the decay becomes increasingly rapid as $J/W\rightarrow(J/W)_c$. Furthermore, one sees from Fig. 7 that η increases as $J/W\rightarrow(J/W)_c$ and never equals $\frac{1}{4}$ as in the usual XY transition.

IV. CONCLUSIONS

Our Monte Carlo calculations clearly show that the "Kondo necklace" does not exhibit long-range magnetic order in its ground state for $0<J/W<2$. In fact, the finite-size scaling analysis of the magnetic structure factor is consistent with a critical point at $J=0$. In this case, for any finite J the magnetic correlations decay exponentially. A similar behavior has been reported by Jullien and coworkers[6] for the 1D Kondo lattice Eq. (1). However, they obtained this result using approximate real-space renormalization-group procedures which predict a finite $(J/W)_c$ ratio for the "Kondo necklace." While we cannot rule out an XY-like phase with algebraic decay for $J/W<(J/W)_c$, the η values are large. Furthermore, the exact two- and four-site results are consistent with the picture that increasing J from 0 immediately decreases correlations along the chain. The ground-state energy of the "Kondo necklace" is evaluated to an estimated error of 0.5%, and a plot of $\langle \mathbf{S}(i)*\tau(i)\rangle$ shows clearly that as the exchange coupling is increased the S and τ spins condense into independent singlets on each site.

ACKNOWLEDGMENTS

This work was supported by the U.S. Department of Energy Grant No. DE-AT03-83ER45008. R.T.S. acknowledges support by the National Science Foundation and numerous fruitful conversations with E. Loh, Jr. We also gratefully acknowledge E. I. du Pont de Nemours and Company and the Xerox Corporation for their support.

[1]See, for example, *Valence Instabilities and Related Narrow Band Phenomena,* edited by R. D. Parks (Plenum, New York, 1977).
[2]S. Doniach, Physica **91B**, 231 (1977).
[3]B. Cornut and B. Coqblin, Phys. Rev. B **5**, 441 (1972).
[4]A. Luther and I. Peschel, Phys. Rev. B **12**, 3098 (1975).
[5]R. Jullien, J. N. Fields, and S. Doniach, Phys. Rev. B **16**, 4889 (1977).
[6]R. Jullien, P. Pfeuty, A. K. Battarcharjee, and B. Coqblin, in Mixed Valence and Magnetism (unpublished).
[7]W. Hanke and J. E. Hirsch, Phys. Rev. B **25**, 6748 (1982).
[8]R. Blankenbecler and R. L. Sugar, Phys. Rev. D **27**, 1304 (1983).
[9]D. Kung, R. Blankenbecler, and R. L. Sugar, Phys. Rev. B (to be published).
[10]D. K. Campbell, T. A. DeGrand, and S. Mazumder, Phys. Rev. Lett. **52**, 1717 (1984).
[11]J. Potvin and T. A. De Grand, Phys. Rev. D **30**, 1285 (1984); R. Blankenbecler and D. Dahl (unpublished).
[12]J. Kuti, Phys. Rev. Lett. **49**, 183 (1982).
[13]J. Kuti and J. Polonyi (unpubished).
[14]R. T. Scalettar (unpublished).
[15]D. M. Ceperley and M. H. Kalos, in *Monte Carlo Methods in Statistical Physics,* edited by K. Binder (Springer, Berlin, 1979), and references contained therein.
[16]Note that before the rotation leading to Eq. (8) this structure factor would have corresponded to an antiferromagnetic structure factor with $Q=\pi$.